Desalination and Water Treatment
www.deswater.com

doi: 10.1080/19443994.2013.803324

52 (2014) 4314–4333
June

Taylor & Francis
Taylor & Francis Group

Quantitative XRD analysis of the dehydration–hydration performance of (Na^+, Cs^+) exchanged smectite

Marwa Ammar, Walid Oueslati*, Hafsia Ben Rhaiem, Abdesslem Ben Haj Amara

UR05/13-01 : Physique des Matériaux Lamellaires et Nanomatériaux Hybrides (PMLNMH), Faculté des Sciences de Bizerte, Zarzouna, 7021, Tunisia
Tel. +21620843705; Fax: +216 72 590 566; email: walidoueslati@ymail.com

Received 17 July 2012; Accepted 2 May 2013

ABSTRACT

The clay mineral membrane is increasingly used, as a natural geological barrier, in wastewater treatment. The variation of the environmental condition (T, P, RH, etc.) induces probably several change on the materials structure. This work aims at characterizing the link between dehydration–hydration behavior, charge location, and the ionic radius, in the case of dioctahedral smectites, exchanged with Na^+ and Cs^+ cation, which are occurred from industrial waste. A natural montmorillonite and beidellite, with different charge location (respectively, dioctahedral and trioctahedral), are selected. The exchange process is directed using Na^+ and Cs^+ cations. The hydration hysteresis is investigated "*in situ*" as a function of relative humidity condition rates. All samples are studied using quantitative X-ray diffraction (XRD) analysis. This method allows us to determine the structural parameters obtained from the theoretical mixed layer structure used to fit experimental XRD patterns. For both Na^+ and/or Cs^+ exchangeable cations, an increase in hydration heterogeneity degree for the tetrahedral substituted smectite layer is noted and the position of exchangeable Cs^+ cation induce a homogeneous hydration trend which is interpreted by a new interlamellar space organization.

Keywords: Disordered systems; Liquid–solid reactions; Crystal structure; X-ray diffraction

1. Introduction

The specific properties of the clays minerals enable them to be potentially used as adsorbents for treating heavy metals and organic pollutants from surface waters, land, or reused mainly originated from the highly polluted effluents and suspended solids present in industrial wastewater, mining operations, and from olive mills. In this context, several studies have presented the concept of coagoflocculation based on the use of clay–polymer nanocomposites to lower the amount of suspended solids. As example: Rytwo et al. [1] examined suitable nanocomposites based on different clays and polymers where the X-ray diffraction (XRD) measurements indicated that sequential addition of olive mill or winery effluents with a boosting dose of nanocomposites may yield a very efficient and rapid clarification pretreatment. Furthermore, Giora [2] presents in his study a nanocomposites, comprised of an anchoring particle and a polymer, as "coagoflocculants" and demonstrates that the use of such particles combines the advantages of coagulant and

*Corresponding author.

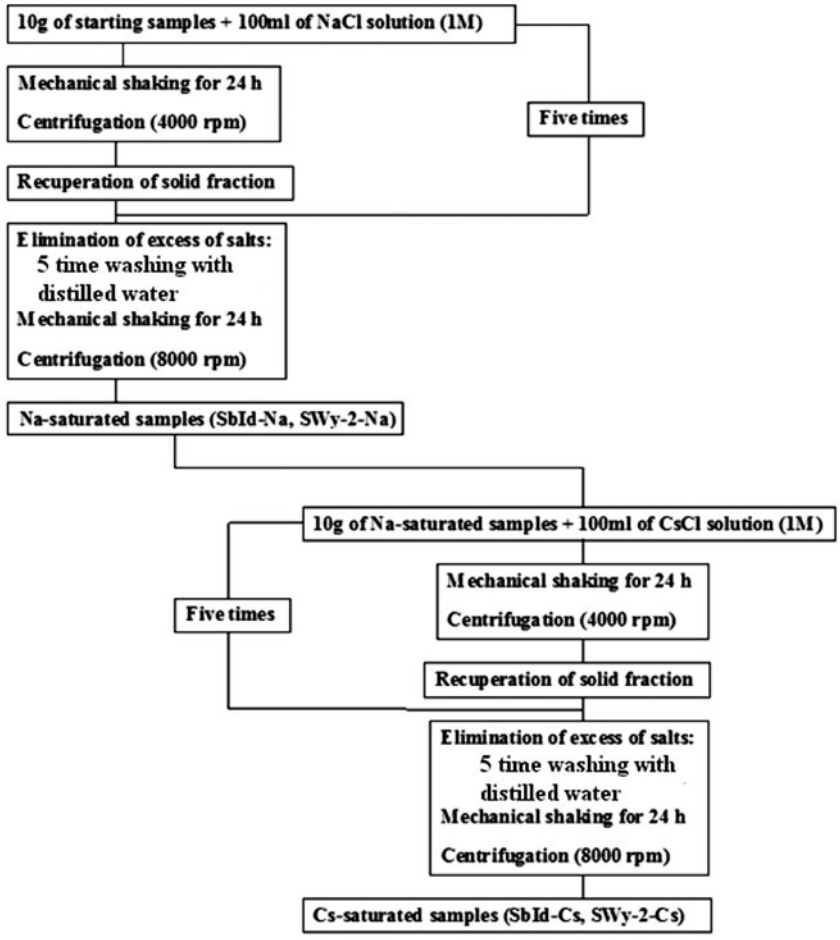

Fig. 1. Experimental protocol of the ionic exchange processes.

flocculant by neutralizing the charge of the suspended particles while bridging between them and anchoring them to a denser particle (the clay mineral), enhancing their precipitation.

Smectite minerals are a basic candidate material used as a natural barrier for wastewater treatment and radioactive waste confinement. Dioctahedral smectites are a 2:1 phyllosilicate with a basic structure consisting of two siliceous tetrahedral sheets sandwiching an octahedral ones, where vacant sites are often occupied by trivalent cation [3–5]. A tetrahedral or octahedral isomorphic cationic substitution defines, respectively, beidellite and montmorillonite subgroups, which induce a charge deficit compensated by exchangeable cations occurring in our study from the soil solutions, containing essentially water and polar molecules and more [6–12].

Also, it is characterized by an important expandability property of its interlayer's spaces, a low permeability, a high specific surface, and elevated nature abundance. Numerous investigations were conducted to study the interaction between smectite and different types of solvents using more than one experimental and theoretical analysis methods.

In the studies of Zamparas et al. [13], modified inorganic clays by Zenith/Fe is used as adsorbent for phosphate removal from natural waters proving that Zenith/Fe is a very good adsorbent for phosphorus removal and potential lake restoration.

Montmorillonite K10 and KSF, modified by polymeric aluminium (Al) or ferric (Fe) and/or Al/Fe mixed polymeric species, was used as coagulants for wastewater treatment were investigated in the study of Ref. [14] where results showed that both modified montmorillonite clays species possess greater properties to remove the particles (as suspended solids) and organic pollutants (as COD and UV254-abs.) from the wastewater.

Malikova et al. [15] studied, using MC and molecular dynamics simulations, the temperature activation of Na/Cs diffusion in montmorillonite and demonstrate that the structural changes are limited to the

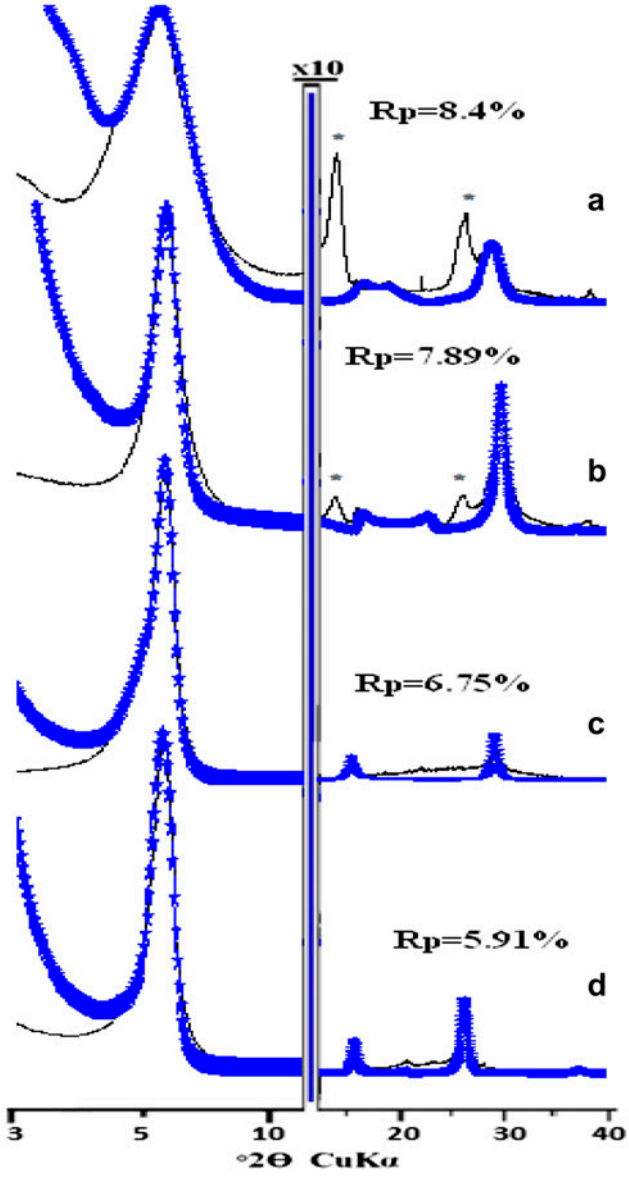

Fig. 2. Comparison between experimental (——) and calculated (*****) XRD patterns (air dry condition). case of : (a)SbI-1-Na, (b) SbI-1-Cs, (c) SWy-2-Na, and (d) SWy-2-Na, (*) supplementary reflexion attributed to 1:1 clay (kolinite).

water phase; marked difference is observed in the modes of diffusion of Cs and Na ions. In the others hand, and based on XRD analysis, [16] investigate the aging processes of copper added to bentonite and the effects of temperature and pH on this processes; they studied the changes of basal spacing of bentonite saturated with Cu at different pH solutions and showed that the d_{001} basal spacing decreases by the augment of pH values from 1.51 nm at pH 4.42 to 1.26 nm at pH 7.68. Zhoua et al. [17] investigates the link between smectite charge location and hydration properties using molecular simulation. They approve that layer-charge distribution is found to have significant influences on the mobility of interlayer species and preference of ion binding sites.

The works of Ref. [18–22] based on XRD analysis, shows the increase of interlamellar space thickness as a function of atmospheric environment (i.e. various relative humidity (RH)). They defined a discrete water sheets organization in the interlamellar space, ascribed respectively to dehydrated (0W, $d_{001} \approx 9.7$–10.2 Å), monohydrated (1W, $d_{001} \approx 11.6$–12.9 Å), bihydrated (2W, $d_{001} \approx 14.9$–15.7 Å), and trihydrated (3W, $d_{001} \approx 18$–19 Å) layers [23].

The present study aims to examine the structural's changes of two dioctahedral smectite (montmorillonite and beidellite samples) as a function of the RH condition. These objectives are directed using an XRD profile modeling approach based on the comparison between the experimental *00l* XRD reflections with calculated ones. This theoretical approach allows us to determine the structural parameter along the c^* axis.

2. Materials and methods

2.1. Starting samples

Based on their specific layer-charge location, two smectites from the Source Clay Minerals Repository Collection [24] are selected as starting materials. The first sample is the beidellite SbId-1 (extracted from Glen Silver Pit, DeLamare Mine, Idaho) characterized by a most isomorphic substitution in tetrahedral sheets with a structural formula [25]:
$(Si^{4+}_{3.772}, Al^{3+}_{0.228})$ $(Al3^{+}_{1.786}, Fe^{3+}_{0.104}, Mg^{2+}_{0.046}, Mn^{3+}_{0.001}, Ti^{4+}_{0.048})$ $(Na^{+}_{0.012}, K^{+}_{0.159})$ (O_{10}) $(OH)_2$

Table 1
Qualitative XRD investigations for all studied samples under "air dry" conditions

Sample	d_{001}(Å)	FWHM(°2θ)	ξ, Xi	Character
SbId-1-Na	12.41	1.82	0.17, 4	l
SbId-1-Cs	12.19	0.83	0.10, 4	H
SWy-2-Na	12.29	0.74	0.15, 4	H
SWy-2-Na	12.36	0.67	0.05, 4	H

Table 2
Structural parameters used for modeling XRD profiles of different studied sample under room conditions

			2W				1W				0W			
Sample	MLS%	2W/1W/0W	L.Th	n_{H_2O}	Z_{H_2O}	$n_{exch.cat}$	$Z_{exch.cat}$	L.Th	n_{H_2O}	Z_{H_2O}	$n_{exch.cat}$	$Z_{exch.cat}$	L.Th	$n_{exch.cat}$	$Z_{exch.cat}$	0W/1W/2W	M
SbId-Na	90	0/65/35—R0	–	–	–	–	–	12.50	1.25	9.70	0.36	10.70	10	0.36	8.60	41.5/58.5/0	4
	10	0/0/100															
SWy-Na	76	0/92/8—R0	15.20	2	10.3/14	0.35	12.80	12.36	1	9.8	0.36	9.80	10.15	0.35	8.50	6/85/9	11
	19	30/70/0—R0															
	5	65/35/0—R0															
SbId-Cs	75	0/90/10—R0	–	–	–	–	–	12.16	2.5	9.50	0.36	9.65	10.20	0.36	9.00	16/84/0	9
	25	0/65/35—R0															
SWy-Cs	100	0/100/0—R0	–	–	–	–	–	12.30	1.5	9.50	0.36	9.30	–	–	–	0/100/0	8

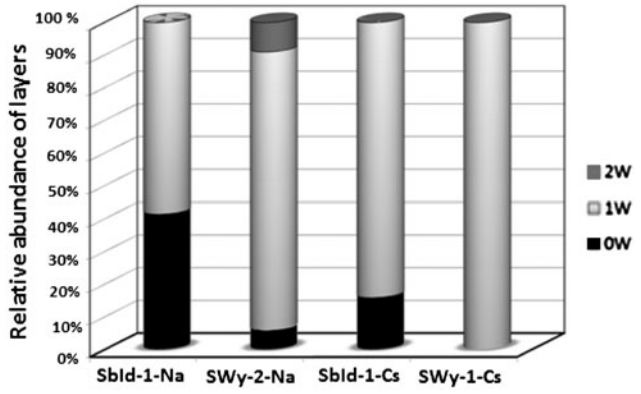

Fig. 3. Relative contribution of the different layer types (summing up all mixed-layer structures) for different samples studied under room conditions.

The second smectite type is the <2 μm fraction of montmorillonite originated from bentonites of Wyoming which exhibits a major octahedral charge and extremely limited tetrahedral substitutions. Its half-cell structural formula that determined by Ref. [26], is as the following:

$$(Si_{3,923}\ Al_{0,077})\ (Al_{1,459}\ Ti^{4+}_{0,018}\ Fe^{3+}_{0,039}\ Fe^{2+}_{0,045}\ Mg^{2+}_{0,382})\ O_{10}(OH)_2(Ca^{2+}_{0,177}\ Na^{+}_{0,027})$$

2.2. Preliminary treatments

To ensure the same experimental conditions for all studied complexes, a sodium exchange, according to the classical protocol [27], is performed. This step is realized in order to guarantee better dispersion for the selected samples.

This process is assured by dispersing, respectively, 10 g)of the beidellite (SbId-1) and montmorillonite (SWy-2) fraction, five times, in 100 ml of 1 N NaCl solution. The suspension is shaken mechanically for 24 h, and then the solid fraction is separated by centrifugation. Removal of the excess salt is performed by washing five times via immersion for 24 h in distilled water. The solid–liquid separation is achieved by centrifugation using SIGMA laboratory centrifuge at 8,000 rpm speed. Resulting samples are hereafter referred to as SbId-1-Na and SWy-2-Na.

2.3. Experimental protocol

The ionic exchange processes were conducted using the following protocol reported in Fig. 1.

For all samples (SbId-1-Na, SbId-1-Cs, SWy-2-Na, and SWy-2-Cs), an oriented glass slides are prepared using the pipette method and then drying at room

Table 3
Qualitative XRD investigations versus relative humidity (RH) conditions

	%RH	d_{001} (Å)	FWHM (°2θ)	ξ, Xi	Character		d_{001} (Å)	FWHM (°2θ)	ξ, Xi	Character
SWy-2-Na	80	16.73	0.63	0.22, 3	H	SWy-2-Cs	13.13	1.68	0.50, 3	I
	70	16.38	1.05	0.40, 3	I		12.77	1.51	0.30, 3	I
	60	15.74	1.55	0.79, 3	I		12.34	1.10	0.10, 3	I
	50	13.75	1.24	0.10, 3	I		12.23	0.87	0.06, 3	H
	40	13.53	0.75	0.08, 3	H		12.17	0.77	0.04, 3	H
	30	13.46	0.78	0.09, 3	H		12.11	0.78	0.05, 3	H
	20	13.36	0.95	0.16, 3	H		11.97	0.97	0.10, 3	H
	10	12.20	2.11	0.18, 3	I		11.60	1.29	0.10, 3	I
	20	12.62	2.29	0.14, 3	I		11.74	1.17	0.40, 3	I
	30	13.62	1.99	0.70, 3	I		11.82	1.14	0.27, 3	I
	40	13.76	1.44	0.10, 3	I		12.16	0.77	0.30, 3	H
	50	13.86	1.71	0.12, 3	I		12.23	0.88	0.07, 3	H
	60	16.27	0.93	0.50, 3	I		12.23	1.00	0.08, 3	H
	70	16.38	0.81	0.51, 3	I		12.43	1.22	0.18, 3	I
	80	16.55	0.60	0.38, 3	H		12.94	1.68	0.60, 3	I
SbId-1-Na	80	14.00	1.85	0.70, 3	I	SbId-1-Cs	11.92	0.94	0.12, 3	H
	70	13.75	1.79	0.80, 3	I		11.92	0.90	0.10, 3	H
	60	13.27	1.77	0.80, 3	I		11.90	0.99	0.17, 3	H
	50	13.11	1.89	0.70, 3	I		11.89	0.88	0.13, 3	H
	40	12.87	1.95	0.70, 3	I		11.87	0.90	0.12, 3	H
	30	12.62	2.14	0.60, 3	I		11.85	0.91	0.13, 3	H
	20	12.03	2.39	0.80, 3	I		11.79	0.90	0.14, 3	H
	10	11.15	2.70	1.40, 3	I		11.15	0.93	0.30, 3	H
	20	11.66	2.60	1.20, 3	I		11.31	1.86	0.38, 3	I
	30	12.60	2.24	0.60, 3	I		11.40	2.01	0.42, 3	I
	40	12.83	2.14	0.42, 3	I		11.47	1.76	0.56, 3	I
	50	13.05	1.81	0.22, 3	I		11.65	1.59	0.16, 3	I
	60	13.75	1.80	0.16, 3	I		11.81	1.08	0.20, 3	I
	70	13.50	1.74	0.16, 3	I		11.86	1.02	0.16, 3	I
	80	13.72	1.77	0.15, 3	I		11.92	0.95	0.14, 3	H

Note: FWHM (°2θ) calculated for (001) reflection, ξ(Å): calculated as the standard deviation of the $\ell \times d(00\ell)$ values for all measurable reflections over the 3–40°2θ angular range, Character: H(homogeneous), I (interstratified).

temperature during a few hours to obtain an air-dried preparation [28].

2.4. XRD study under controlled atmosphere

The XRD patterns are recorded using BRUKER D8 Advance diffractometer using CuKα1 monochromatic radiation and monitored by EVA release software. The diffractometer installation is equipped with an Ansyco rh-plus 2,250 humidity control device coupled to an Anton PaarTTK450 chamber. Intensities are measured at the angular range 3–40 °2θ. The usual scanning parameters are 0.04 °2θ as step size and 6 s as counting time per step over the angular range 2–50° 2θ. The divergence slit, the two solar slits, the antiscatter, and resolution slits were 0.5°, 2.3°, 2.3°, 0.5°, and 0.06°, respectively. All studied samples are recorded initially under room condition (air dry condition). After that, they are studied under controlled atmosphere. Indeed, the RH values decreases from 80% RH to the extremely dry ones (10% RH) in first sequence, followed by a gradual increase, starting from 20% RH to 80% RH. The experimental XRD patterns are recorded every 10% RH scale at the fixed RH condition values along the dehydration–hydration cycle.

2.4.1. Qualitative XRD patterns investigations

The qualitative XRD analysis consists in the investigation of the *00l* basal reflection position and peak shape (d_{00l} basal spacing values, peak symmetry, and/

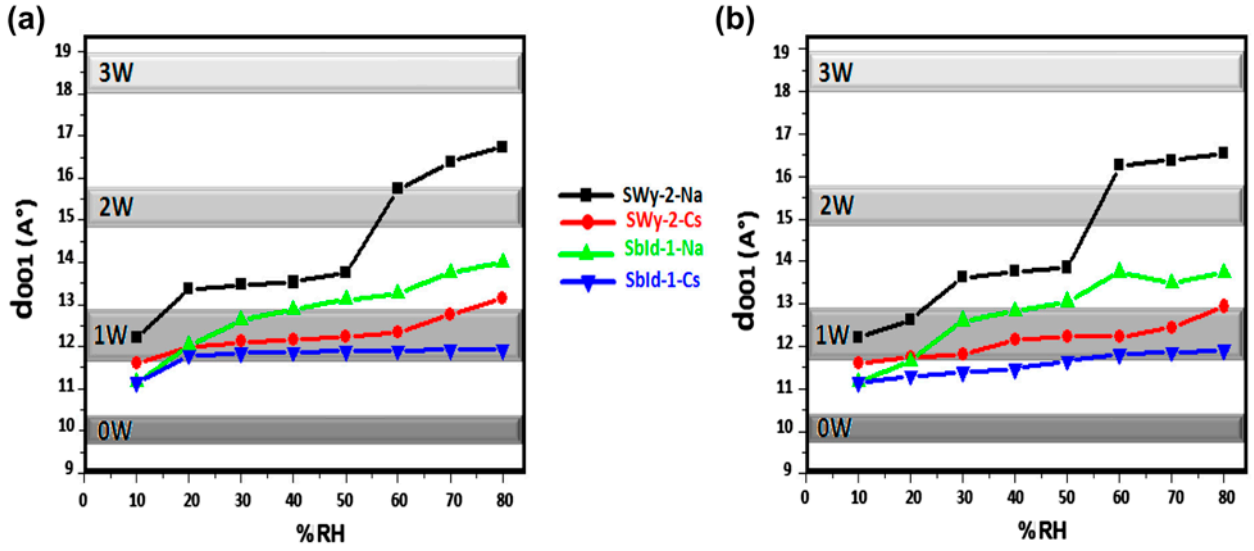

Fig. 4. Evolution of the d001 basal spacing value versus %RH rate along dehydration (a) and hydration (b) process.

or asymmetry). Furthermore, we can use the full width at half maximum intensity (FWHM) for *001* reflection and the irrationality (ξ) parameter [29], which is calculated as the standard deviation of the $l \times d(00l)$ values calculated for all *Xi* measurable reflections (i.e. $Xi \leqslant 5$ measurable reflections) over the explored $2\theta^{\circ}$ angular range. Nevertheless, these qualitative examinations remains insufficient to determine the evolution of different structural parameters, such as the position and organization of exchangeable cations with water molecule in the interlamellar space along the c^* axis.

2.4.2. Quantitative XRD analysis

The quantitative study is based on the modeling of *00l* reflections for different samples, performed using the algorithms developed by [30]. This method consists of comparing the experimental patterns with the theoretical intensities calculated according to the matrix formalism given by Drits and Tchoubar [31]. The XRD patterns are calculated using the z-coordinates of [32]. The origin of these coordinates was placed on the plane of surface oxygen atoms [33]. The modeling of XRD patterns is accomplished using the fitting strategy described by [33,34] which consists of reproducing the experimental XRD pattern using a main structure with only one type of layer if possible, and if necessary, additional contributions of a mixed layer structure MLSs to the diffracted intensity, are introduced in order to achieve the optimum agreement between calculated and experimental patterns. The abundances (Wi), the mode of stacking of the dif-

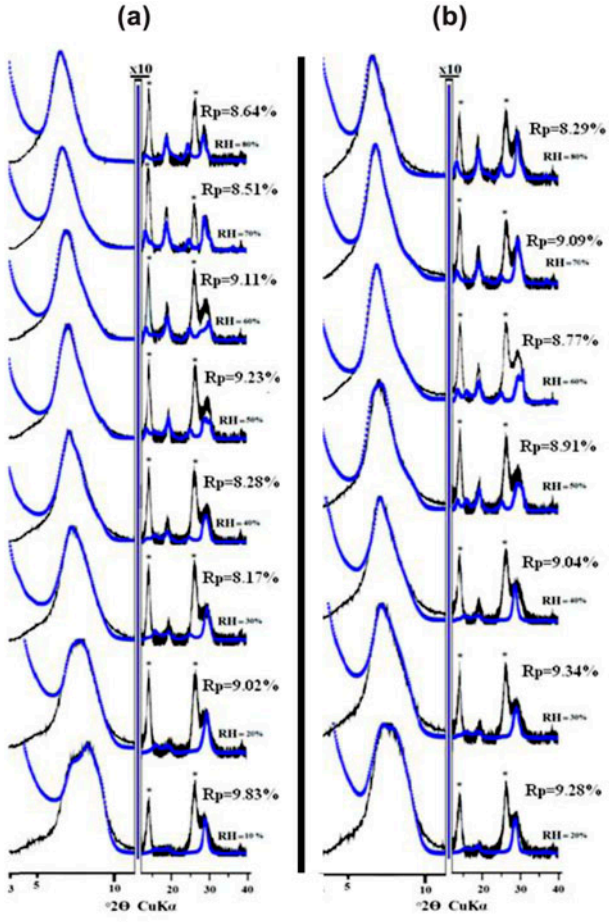

Fig. 5. Comparison between experimental (——) and calculated XRD patterns (****) as a function of %RH, along the dehydration (a) and hydration (b) process, in the case of SbId-1- Na. (*) supplementary reflection due to 1:1 clay (Kaolinite).

Table 4
Structural parameters used to reproduce experimental patterns of SbId-1-Na as a function of RH along the dehydration–hydration process

% RH	L.T 2W	n_{H_2O} 2W	Z_{H_2O} 2W	n_{Na} 2W	Z_{Na} 2W	L.T 1W	n_{H_2O} 1W	Z_{H_2O} 1W	n_{Na} 1W	Z_{Na} 1W	L.T 0W	n_{Na} 0W	Z_{Na} 0W	Total 0W/1W/2W	*M*
80	15	10	10/14	0.36	12.90	12.65	3	9.50	0.36	9.50	10.00	0.36	8.00	12.00/54.27/33.73	8
70	14.80	10	9.5/14	0.36	12.80	12.45	1.8	9.40	0.36	9.40	9.65	0.36	8.00	21.88/52.82/25.30	8
60	14.60	10	9.6/13.9	0.36	12.80	12.15	1.8	9.60	0.36	9.20	9.90	0.36	8.00	28.26/49.06/22.68	11
50	14.60	10	9.6/13.9	0.36	12.50	12.15	1.5	9.70	0.36	9.00	9.65	0.36	8.20	36.62/47/16.38	10
40	14.65	8	9.8/14	0.36	12.60	12.20	1.5	9.50	0.36	9.50	9.65	0.36	8.00	37.98/50.52/11.50	12
30	14.50	7.4	10.5/14	0.36	12.60	12.00	1.4	9.00	0.36	9.00	9.50	0.36	8.00	42.80/49/8.20	10
20	14.20	7	10.4/13.8	0.36	12.60	12.00	1.4	9.00	0.36	9.00	9.50	0.36	8.00	60.37/37.78/1.85	9
10	14.20	7	10.4/13.8	0.36	12.60	12.00	1.4	9.00	0.36	9.00	9.50	0.36	8.00	65.30/33.45/1.25	9
20	14.90	7	10.4/13.8	0.36	12.40	12.40	1.4	9.00	0.36	9.10	9.70	0.36	8.10	60.67/37.10/2.23	8
30	14.40	7.2	9.3/14	0.36	12.60	12.20	1.6	9.60	0.36	9.60	9.65	0.36	8.00	53.65/42.90/3.45	8
40	14.70	7.8	9.5/13.8	0.36	12.60	12.45	1.6	9.60	0.36	9.60	9.70	0.36	8.20	50.47/45.78/3.75	8
50	14.50	8.5	9.7/14	0.36	12.80	12.00	1.6	9.70	0.36	9.70	9.50	0.36	8.20	42/44.50/13.50	12
60	14.60	9	9.5/13.9	0.36	12.50	12.00	2.2	9.90	0.36	9.90	9.50	0.36	8.10	33.82/48.36/17.82	12
70	14.70	9	9.5/13.9	0.36	12.50	12.25	3	9.30	0.36	9.70	9.60	0.36	8.00	30.95/51.85/17.20	10
80	14.65	10.4	9.6/14	0.36	12.70	12.30	3.5	9.30	0.36	9.30	9.60	0.36	8.00	15.75/59.50/24.75	8

Note: 2W, 1W, and 0W attributed to the layer hydration state. (Layer thickness (LT in Å). *n*: number of H_2O molecules for hydrated layers (per O_{20} $(OH)_4$). *Z*: position of H2O molecule along the c^* axis. *n*: number of exchangeable cations per half unit cell. *Z*: position of exchangeable cations per half unit cell calculated along c^* axis.) respectively for 2W, 1W, and 0W and M: average layer number per stacking.

ferent kinds of layers, and the average number of layers per coherent scattering domain (CSD) [31] can be determined also from this theoretical method. Within a CSD, the stacking of layers is described by a set of junction probabilities (*Pij*).

2.4.3. Theoretical water molecule distribution

Smectites have the best swelling properties which depend on the layer charge, charge location (octahedral vs. tetrahedral), the nature of exchangeable cations, the CEC (i.e. Cation Exchange Capacity), and the specific surface value. It is controlled by the balance between repulsive forces between neighboring 2:1 layers and attractive forces between hydrated interlayer cations and the negatively charged surface of their 2:1 layers [35–41].

Based on XRD analysis, the expansion characteristics under variable RH rates is widely studied [21–23,42–46] revealing that the position of *00l* basal reflections, which is shifted from the high angular 2θ range towards small ones, varied with the interlamellar water content. By increasing of %RH amounts, smectite expands stepwise, with the different steps corresponding to the insertion of 0, 1, 2, or 3 sheets of H_2O molecules in the interlayer space easily detected by XRD by an increase in basal spacing.

Table 5
Structural parameters used to reproduce experimental patterns of SWy-2-Na as a function of %RH rates

			2W					1W					0W				
%RH	MLS%	2W/1W/0W	L.Th	n_{H_2O}	Z_{H_2O}	n_{Na}	Z_{Na}	L.Th	n_{H_2O}	Z_{H_2O}	n_{Na}	Z_{Na}	L.Th	n_{Na}	Z_{Na}	0W/1W/2W	*M*
80	71.25	80/20/0—R0	15.35	5.8	10.50/14.10	0.35	12.80	12.45	2.9	9.00	0.35	9.00	–	–	–	0/32/68	11
	23.75	45/55/0—R0															
	5	95/05/0—R0															
70	52.70	70/30/0—R0	15.35	5.6	0.80/14.10	0.35	12.80	12.40	2.8	9.00	0.35	9.00	10.30	0.35	8.20	0.75/52.65/46.60	11
	32.30	30/70/0—R0															
	15	0/95/05—R0															
60	26	65/35/0—R0	15.20	5.6	9.80/14.00	0.35	12.70	12.40	2.8	9.70	0.35	9.70	10.20	0.35	8.30	3.50/67.90/28.60	10
	39	30/70/0—R0															
	35	0/90/10—R0															
50	14.35	55/45/0—R0	15.20	3.9	10.20/14.00	0.35	12.70	12.35	1.95	9.80	0.35	9.80	10.20	0.35	8.20	7.70/79.10/13.20	12
	26.65	20/80/0—R0															
	59	0/87/13—R0															
40	18.80	25/75/0—R0	15.20	3.6	10.20/14.00	0.35	12.60	12.30	1.8	9.70	0.35	9.70	10.20	0.35	8.00	9/83/8	11
	75.20	0/88/12—R0															
	6	55/45/0—R0															
30	77.60	0/88/12—R0	15.20	3	10.00/14.00	0.35	12.60	12.30	1.5	9.70	0.35	9.70	10.20	0.35	8.20	9.30/83.20/7.50	12
	19.40	30/70/0—R0															
	3	55/45/0—R0															
20	69.6	0/80/20—R0	15.20	3	10.00/14.00	0.35	12.50	12.26	1.5	9.70	0.35	9.50	10.20	0.35	8.00	21.75/75/3.25	10
	17.4	0/55/45—R0															
	13	25/75/0—R0															
10	66.50	0/65/35—R0	15.40	2.4	10.00/14.00	0.35	12.40	12.15	1.2	9.70	0.35	9.70	9.70	0.35	8.00	58.90/40.60/0.50	7
	28.50	0/45/55—R0															
	5	10/90/0—R0															
20	78.20	0/40/60—R0	15.60	2.4	10.30/14.20	0.35	12.50	12.25	1.2	9.70	0.35	9.70	9.65	0.35	8.10	52.44/46.36/1.20	7
	13.80	0/60/40—R0															
	8	15/85/0—R0															
30	81.60	0/65/35—R0	15.00	2.6	10.00/14.00	0.35	12.60	12.25	1.3	9.70	0.35	9.60	9.95	0.35	8.20	28.56/66.24/5.20	6
	14.40	25/75/0—R0															
	4	40/60/0—R0															
40	32.85	30/70/0—R0	15.20	4.4	10.20/14.00	0.35	12.70	12.30	1.8	9.70	0.35	9.70	10.20	0.35	8.20	2.75/79.50/17.75	11
	55	0/95/05—R0															
	12.15	65/35/0—R0															
50	24.80	65/35/0—R0	15.20	5	10.20/14.00	0.35	12.80	12.40	2	9.30	0.35	9.50	10.20	0.35	8.30	3.8/68.9/27.30	10

(*Continued*)

Table 5 (*continued*)

%RH	MLS%	2W/1W/0W	2W				1W				0W			0W/1W/2W	M
			L.Th	n_{H_2O}	Z_{H_2O}	n_{Na}	Z_{Na}	L.Th	n_{H_2O}	Z_{H_2O}	n_{Na}	Z_{Na}	L.Th	n_{Na}	Z_{Na}		
	37.20	30/70/0—R0															
	38	0/90/10—R0															
60	63	35/65/0—R0	15.00	5.6	10.50/14.00	0.35	12.80	12.40	2.8	9.70	0.35	9.60	10.20	0.35	8.20	2.25/47.95/49.80	9
	27	25/75/0—R0															
	10	0/90/10—R0															
70	69	70/30/0—R0	15.35	5.6	10.35/14.10	0.35	12.90	12.40	2.8	9.00	0.35	9.30	10.30	0.35	8.00	1.2/44.75/54.05	10
	23	25/75/0—R0															
	8	0/85/15—R0															
80	85	75/25/0—R0	15.45	5.8	10.50/14.20	0.35	12.90	12.45	2.8	9.00	0.35	9.50	–	–	–	0/33.25/66.75	12
	15	0/80/20—R0															

3. Results

3.1. Study under room conditions (reference sample)

3.1.1. Qualitative XRD analysis

The XRD patterns produced by all samples studied under room conditions are reported in Fig. 2. In the case of **SbId-1-Na** and **SbId-1-Cs**, a supplementary reflections attributed to the presence of a 1:1 clay mineral fraction (Kaolinite) in starting sample (i.e. SbId-1) are shown.

The d_{001} basal spacing values, the FWHM of the 001 reflection, and the ξ parameter are calculated for all experimental patterns and they are illustrated in Table 1.

XRD patterns produced by **SbId-1-Na** sample presents a *001* reflection situated at $2\theta = 7,\ 12^{\circ}$ ($d_{001} = 12,\ 41$ Å) (Fig. 2(a)) and characterized by an asymmetric peaks profile accompanied by a high ξ and FWHM value (i.e. 0.17 Å and 1.82) indicating a heterogeneous hydration character.

For **SbId-1-Cs**, the XRD pattern (Fig. 2(b)) present a *001* basal reflection situated at $2\theta = 7,\ 26^{\circ}$ ($d_{001} = 12,\ 19$ Å) attributed to "1W" hydration state phase [23]. The ξ and FWHM values (i.e. 0.10 Å and 0.83) show a rational series of the *00l* reflection positions confirmed with the symmetric peaks shapes, which indicate a homogeneous hydration state character.

On the other hand, for **SWy-2-Na** complex, the *001* reflection is situated at $2\theta = 7.18^{\circ}$ ($d_{001} = 12,\ 29$ Å) (Fig. 2(c)) characterizing the "1W" hydration state [23]. According to Ref. [21], the calculated values of the ξ and FWHM which are, respectively, 0.15 A°and 0.74°, assign the quasi-homogeneous hydration character.

The XRD pattern related to **SWy-2-Cs** sample is characterized by $d_{001} = 12.36$ Å indicating the insertion of one water sheet in the interlamellar space. The peaks' symmetry description, ξ parameter, and FWHM value (i.e. 0.23 Å and 0.67) confirm the obtained rational reflections series and indicate the homogeneous hydration state character [33].

3.1.2. Quantitative XRD analysis

The theoretical XRD model related to **SbId-1-Na** sample is obtained using two MLSs types. The first layer type is composed by (1W:0W at 55:45 ratio, respectively) mixed with a second one characterized by (1W:0W at 80:20 ratio, respectively). For **SbId-1-Cs sample**, the best fit is achieved using two MLSs types exhibiting random interstratification between 1Wand 0W layers. For the monohydrated layer, the H_2O molecules sheets are located at 9.50 Å along the c^* axis and the exchangeable cation (i.e. Cs^+) is placed at

Table 6
Structural parameters used to reproduce experimental patterns of SbId-1-Cs as a function of RH along the dehydration–hydration process

% RH	L.T 2W	n_{H_2O} 2W	Z_{H_2O} 2W	n_{Cs} 2W	Z_{Cs} 2W	L.T 1W	n_{H_2O} 1W	Z_{H_2O} 1W	n_{Cs} 1W	Z_{Cs} 1W	L.T 0W	n_{Cs} 0W	Z_{Cs} 0W	Total 0W/1W/2W	*M*
80	–	–	–	–	–	12.10	2.8	9.55	0.36	9.70	10.00	0.36	8.50	28/72/0	10
70	–	–	–	–	–	12.10	2.8	9.60	0.36	9.60	10.00	0.36	8.70	28/72/0	10
60	–	–	–	–	–	12.15	2.7	9.70	0.36	9.65	10.00	0.36	8.70	28.75/71.25/0	10
50	–	–	–	–	–	12.10	2.7	9.75	0.36	9.50	9.95	0.36	8.70	31.25/68.75/0	7
40	–	–	–	–	–	12.10	2.5	9.60	0.36	9.70	9.90	0.36	8.50	31.50/68.5/0	9
30	–	–	–	–	–	12.05	2.5	9.60	0.36	9.70	9.85	0.36	8.50	32.60/67.40/0	9
20	–	–	–	–	–	12.05	2.2	9.6	0.36	9.60	9.85	0.36	8.20	37.50/62.50/0	9
10	–	–	–	–	–	12.00	1	9.40	0.36	9.40	9.80	0.36	8.20	67/33/0	9
20	–	–	–	–	–	12.00	1.5	9.45	0.36	9.50	9.80	0.36	8.10	56/44/0	10
30	–	–	–	–	–	12.00	2	9.60	0.36	9.80	9.80	0.36	8.10	54.63/45.37/0	10
40	–	–	–	–	–	12.00	2.2	9.70	0.36	9.70	9.80	0.36	8.20	52.25/47.75/0	10
50	–	–	–	–	–	12.10	2.2	9.80	0.36	9.60	9.90	0.36	8.40	50.25/49.75/0	9
60	–	–	–	–	–	12.10	2.4	9.50	0.36	9.70	9.90	0.36	8.50	40.75/59.25/0	9
70	–	–	–	–	–	12.10	2.7	9.60	0.36	9.60	9.90	0.36	8.40	32/68/0	9
80	–	–	–	–	–	12.15	2.7	9.70	0.36	9.70	9.85	0.36	8.30	31.25/68.75/0	9

Note: 2W, 1W, and 0W attributed to the layer hydration state. (Layer thickness (LT in Å). *n*: number of H_2O molecules for hydrated layers (per O_{20} $(OH)_4$). *Z*: position of H_2O molecule along the c^* axis. *n*: number of exchangeable cations per half unit cell. *Z*: position of exchangeable cations per half unit cell calculated along c^* axis.) repectively for 2W, 1W, and 0W and *M*: average layer number per stack.

$Z_{Cs} = 9.65$ Å. For the 0W layers, the Cs^+ cation is located at 9 Å. The theoretical model of **SWy-2-Na** sample shows the presence of four types of MLS characterized by different hydration state (2W, 1W, and 0W), randomly distributed. The total proportions of these layers are as follows; 2W:1W:0W ratio 9:85:6 and the average number of layers per stack is 11. For **SWy-2-Cs** complex, the quantitative analysis confirms the qualitative ones , in fact, the experimental XRD pattern is reproduced using one homogeneous phase containing 1W layer with an average of eight layer per stacking. All structural parameters used in the simulations are illustrated in Table 2 and the relative proportions of different mixed layer types (summing up all mixed layer structures), deduced from the quantitative study, are reported in Fig. 3.

3.2. Study under controlled RH conditions

All parameters deduced from the qualitative XRD investigation for different complexes are calculated and illustrated in Table 3. In order to predict the layer types present in structure of different samples along the dehydration–hydration process, we present in Fig. 4 the evolution of d_{001} basal spacing value deduced from the *001* reflection positions, for different samples, as function as the %RH rate throughout the dehydration (a) and the hydration (b) process.

3.2.1. Case of Na-saturated samples

3.2.1.1. SbId-1-Na sample. Qualitative XRD analysis: In the case of **SbId-1-Na** complex, all experimental XRD patterns (Fig. 5) are characterized by an asymmetric *001* reflection with a relative high FWHM value and an irrationality for all measurable reflection positions justified by the high ξ parameter values signifying heterogeneous hydration character [29] (Table 3). The evolution of the *001* reflection related to SbId-1-Na vs. RH rates, (Fig. 4) showed a slow increase of interlamellar water content and the structure present,

over the all investigated RH field, three major hydration domains.

Indeed, along the dehydration process, the d_{001} values decrease from 14Å at 80%RH to 13.11Å at 50% RH; this value was probably recognized to an intermediate hydration character including 1W and 2W layers. From 40 to 20% RH, the structure is dominated by monohydrated layer. At 10%RH, d_{001} decline to 11.15 Å indicating a heterogeneous hydrated state between 1W and 0W layers. By increasing RH values to 20% RH, d_{001} expand to 11.66 Å attributed to layer interstratifications exhibiting two hydration states (1W and 0W) with a major proportion of monohydrated layers. Between 30 and 40% RH, the *00l* basal spacing values shift from 12.60to 12.83 Å, which indicates that samples present a quasi-homogeneous 1W hydration state. From 50 to 80% RH, global structure is characterized by an intermediate hydrated state between 1W and 2W. We note that the maximum d_{001} value 13.72 Å is obtained at 80% RH.

Quantitative XRD analysis. *Dehydration process*: The experimental XRD patterns recorded at **80% RH** is modeled using four different contributions consisting, respectively, of two homogeneous 1W and 2W layers phases and two mixed layer structure—2W:1W ratio with 45:55 and 1W:0W ratio with 60:40. Hence, the global structure of the tetrahedral substituted smectites is characterized by the presence of the three layer types (i.e. 2W, 1W, and 0W), respectively, with 33.73, 54.27 and 12% contributions. The number of layers per stacking is 8. Only three contributing structures are needed to fit the obtained experimental profiles recorded at **70% RH**, the first contribution incorporates 1W and 2W layers (2W:1W ratio with 45:55 ratio) whereas the others MLSs present different proportions of 1W and 0W layers. The full structural composition includes 2W:1W:0W ratio with 25.3:52.82:21.88 abundances. At **60% RH,** the theoretical model includes four interstratified structures by combining three homogeneous hydration states (bihydrated, monohydrated, and dehydrated). The decrease of the RH value from **50** to **30%** is accompanied by a progressive "growth" of the 0W layer proportion to the detriment of the dehydrated layer type. In whole, the smectite presents three varying mixed structures vs. the RH value. From 50 to 20%RH, the global structure is modeled using three types of layer (i.e. 2W, 1W, and 0W). The theoretical model presents a heterogeneous structure dominated by the dehydrated layer with 60.37% abundance, 37.78% of monohydrated layer, and a lower relative proportion of bihydrated layer (1.85%). At **10% RH**, four mixed-layer structures were used to reproduce the experimental XRD patterns. Quantitative study shows that the 0W layers abundance increases in the structure at the expense of 1W layers and 2W layers (2W:1W:0W ratio 1.25:33.45:65.3). The number of layers per stack is 9 and all optimum structural parameters used to fit XRD profiles are summarized in Table 4.

Hydration process: Due to the structure heterogeneities observed at **20% RH**, up to four mixed-layer structures, dominated by the dehydrated phases (60.67%), are necessary to reproduce the experimental patterns. A slow evolution in structural **properties** is observed at **30–40% RH** characterized by a low decreasing of the dehydrated layers proportion. Indeed, for 30%RH, the proposed model includes 2W:1W:0W ratio with 3.45:42.9:53.65 abundance, whereas at 40%RH, the structure presents 2W:1W:0W ratio with 3.75:45.78:50.47. Only two MLS are needed to fit the obtained experimental profiles recorded at **50% RH**. The first MLS consist of an arrangement between 0W and 1W hydration states with a major proportion of dehydrated layers (60%) whereas the second contribution incorporates 55 and 45%, respectively, for 1W and 2W layers. **At 60% RH,** the hydration heterogeneity increases, this required an enhancement of mixed-layer contributions number uses for modeling. Such hydration heterogeneity is systematically observed at **70% RH** where the best fitting of the experimental 00*l* reflections is performed assuming four various mixed-layer structures. Summarily, the structure presents 2W:1W:0W ratio with 17.82:48.36:33.82 and 2W:1W:0W ratio with 17.20:51.85:30.95, respectively, at **60% RH** and **70% RH**. By increasing the RH rate to **80%,** hydration heterogeneity disappears. Indeed calculation is performed using just tow MLS including 2W, 1W, and 0W layers with variable amounts. In global, the relative proportion of the dehydrated layers (0W) decreases to15.75% while the abundance of the monohydrated and dehydrated layers increases respectively to 59.50 and 24.75%. The 0W, 1W, and 2W layers compositions and the relative proportions of the different mixed layer structures used in modeling are illustrated in Table 4.

3.2.1.2. SWy-2-Na sample. Qualitative XRD description: The qualitative observation of experimental XRD patterns related to SWy-2-Na sample shows that the major part of the *001* reflection is characterized by an asymmetric peak profiles accompanied with a "shoulder" which indicates the appearance of new hydration phases, except at the higher RH condition in both dehydration and hydration process, the shoulder disappear and the *001* reflections become more symmetric signifying a new homogenous hydration trend (Fig. 6, Table 5). The evolution of the d_{001} as function

Table 7
Structural parameters used to reproduce experimental patterns of SWy-2-Cs as a function of RH along the dehydration–hydration process

% RH	L.T 2W	n_{H_2O} 2W	Z_{H_2O} 2W	n_{Cs} 2W	Z_{Cs} 2W	L.T 1W	n_{H_2O} 1W	Z_{H_2O} 1W	n_{Cs} 1W	Z_{Cs} 1W	L.T 0W	n_{Cs} 0W	Z_{Cs} 0W	T OTAL 0W/1W/2W	*M*
80	14.90	2	9.30/14.00	0.36	12.50	12.30	1	9.00	0.36	9.00	10.30	0.35	8.80	14/70.50/15.50	8
70	14.90	2	9.30/14.00	0.36	12.50	12.30	1	9.00	0.36	9.00	10.30	0.35	8.80	25.50/68.50/6	6
60	15.20	1.6	10.50/14.00	0.36	12.40	12.20	0.7	8.50	0.36	8.90	10.20	0.35	8.00	16.80/79/4.2	8
50	–	–	–	–	–	12.20	0.7	9.00	0.30	9.00	10.40	0.30	8.60	15/85/0	8
40	–	–	–	–	–	12.20	0.7	9.00	0.30	9.00	10.40	0.30	8.60	18/82/0	9
30	–	–	–	–	–	12.23	0.65	9.00	0.28	9.00	10.40	0.28	8.70	20/80/0	10
20	–	–	–	–	–	12.25	0.5	9.00	0.30	9.20	10.35	0.30	8.85	35/65/0	9
10	–	–	–	–	–	12.10	0.4	9.20	0.36	9.70	10.35	0.27	9.00	55/45/0	7
20	–	–	–	–	–	12.30	0.4	9.20	0.36	9.70	10.35	0.27	9.00	55.75/44.25/0	8
30	–	–	–	–	–	12.30	0.5	9.40	0.36	10.20	10.35	0.35	9.00	52.25/47.75/0	8
40	–	–	–	–	–	12.30	0.6	9.50	0.36	10.20	10.35	0.35	9.00	50.50/49.50/0	8
50	–	–	–	–	–	12.28	0.7	9.50	0.36	10.15	10.50	0.35	8.90	20/80/0	9
60	–	–	–	–	–	12.30	0.7	9.20	0.30	10.30	10.20	0.35	8.50	18/82/0	8
70	–	–	–	–	–	12.20	0.8	9.20	0.27	10.00	10.30	0.35	8.70	10/90/0	6
80	15.40	1.6	10.00/14.00	0.36	12.70	12.20	0.9	9.20	0.33	10.00	10.30	0.35	8.70	16.50/79.50/4	6

as RH condition (Fig. 4) showed that, the SWy-2-Na complex is characterized by a rapid evolution on the hydration behavior from homogeneous phases to heterogeneous ones through the intermediate hydration state. The **dehydration process** is characterized by three major hydration phases associated to three ranges of RH values. Indeed, from 80 to 60%RH, the d_{001} value varied from 16.73 to 15.74 Å which means the presence of a major contribution of 2W layer in structure. From 50% RH, a slow evolution of the d_{001} towards 13.36 Å at 20% RH is observed. This d_{001} value is ascribed probably to an interstratified "1W-2W" hydration character. Finally, at 10% RH, the basal spacing value (d_{001} = 12.20 Å) indicates that sample presents a homogeneous 1W hydrated state. Along the **hydration process**, three major hydration states types were observed (i.e. from 10 to 80% RH). From 10 to 20% RH, the sample is characterized by 1W hydration state. From 30% RH to 50RH %, a slow increase of the d_{001} spacing values is observed (i.e. From 13.62 to 13.86 Å) indicating the coexistence of an intermediate 1W–2W hydrated state. An important alteration of the d_{001} basal spacing value was perceived at 60% RH which increases to 16.27 Å and continues its growth until it expects 16.55 Å at 80% RH condition. Thus all over this range of RH values, structure is dominated by the 2W layers type.

Quantitative XRD description. *Dehydration process*: The dehydration process begins from **80% RH** where the obtained experimental XRD pattern is simulated assuming three types of MLSs including 1W and 2W layers with different proportion. The proposed model includes, in total, a major proportion of the bihydrated layers (2W:1W ratio 68:32). **From 70 to 20% RH,** it is possible to reproduce the experimental XRD pattern using three hydration states types (dehydrated.0W, monohydrated.1W, and bihydrated 2W). All structural parameters used to reproduce the experimental profiles are reported in Table 5. At **10%RH,** a notable change in the coexisting relative proportions of 0W, 1W, and 2W layers is noted. In fact, the modeling of the experimental XRD patterns shows a dominance of the dehydrated layers (58.9%) which is the highest proportion detected along the dehydration process for the 0W layers. On the other hand, a low abundance (0.5%) of the bihydrated layers is noted. All structural parameters that made it possible to obtain the best agreement between calculated and experimental XRD patterns are summarized in Table 5.

Hydration process: Experimental XRD patterns recorded at **20% RH and 30% RH** is reproduced using random layer-type interstratifications (i.e. 2W, 1W, and 0W). The total proportions of these layers are as follows 1.2(2W):46.36(1W):52.44(0W) and 5.2(2W):

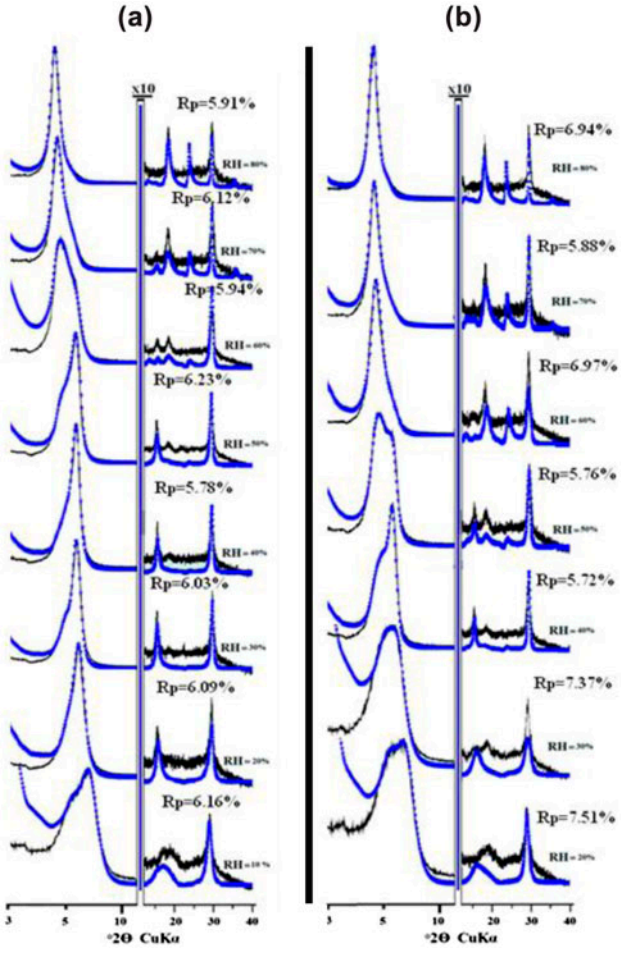

Fig. 6. Best agreement between theoretical (****) and experimental (——) XRD pattern for all measured %RH rates along the dehydration (a) and hydration (b) process of SWy-2-Na.

66.24(1W):28.56(0W), respectively, for XRD patterns related to 20%RH and 30%RH. (Fig. 6(b)). From **40 to 50% RH**, the H_2O sheets insertion becomes easier which facilitates the 0W–1W and 1W–2W transitions. The quantitative study showed an increasing in the relative proportion of bihydrated (2W) and monohydrated layers at the expense of dehydrated layers (0W). For **50% RH, t**he optimum structure model is described using three types of MLS; the first types contain essentially (65%) of 2W and (35%) of 1**W** layers. The second population is composed by 30% of 2W and 70% of 1W layers. The third one presents 90% of monohydrated layers and 10% of dehydrated phases. By increasing RH rate to **70% RH**, a decrease of the 0W layers abundance is observed. The theoretical model is characterized by 49.8%(2W):47.95% (1W):2.25%(0W) and 54.05(2W):44.75(1W):1.2(0W) ratio, respectively, at **60 and 70% RH.** For the extreme % RH conditions **(80% RH),** the structure is characterized by a logical disappearance of the dehydrated layer (i.e.0W). Only two types of MLS including 1W and 2W layer randomly distributed are used to fit experimental data. The relative proportions of the different layers type are as follows 75(2W):25(1W) and 20 (2W):80(1W) ratio. All structural parameters used in the simulation are summarized in Table 5.

3.2.2. *Case of Cs-saturated samples*

3.2.2.1. SbId-1-Cs sample. Qualitative XRD analysis: For SbId-Cs, the observed XRD patterns (Fig 7) and the examined ξ and FWHM value showed that, along the dehydration process, the structure is characterized by a homogenous hydration state character. By increasing RH values, an interstratified hydration state is observed, except at 80% RH, where structure presents a homogenous hydration character. The

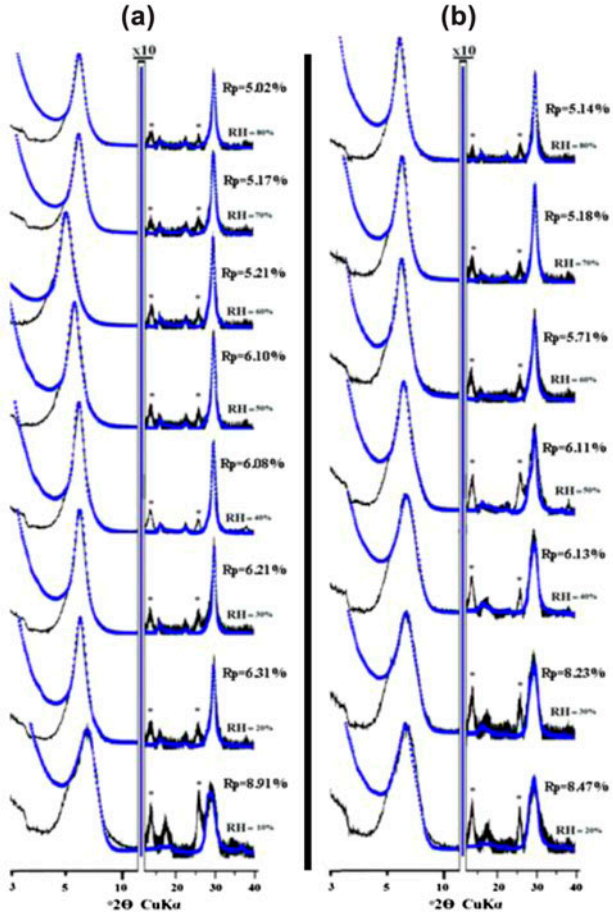

Fig. 7. Comparison between experimental (——) and calculated XRD patterns (****) as a function of RH, along the dehydration (a) and hydration (b) process, in the case of SbId-1-Cs. (*) supplementary reflection of 1:1 clay (Kaolinite).

evolution of the d_{001} vs. % RH rates (Fig. 4) shows an exceptional hydration behavior comparing to others complex. Indeed, the evolution of d_{001} is very slowly especially along the dehydration process, in fact, from 80 to 20% RH, the d_{001} decrease from 11.92 to11.79 Å and the smectite fraction is dominated by the 1W layer hydration state, a simple shift is observed at 10% RH were d_{001} values decrease to 11.15 Å indicating an interstratifications between 0W and 1W layers. Along the hydration process and from 10 to 50% RH, the d_{001} basal spacing shift from 11.15 to 11.65 Å attributed probably to an interstratified character between "0W and 1W" hydration state. Beyond 50% RH, the structure is characterized by the dominance of the monohydrated layers.

Quantitative XRD analysis. *Dehydration process*: The XRD patterns related to **80%RH towards 60%RH** are reproduced assuming coexisting of two MLSs contributions with a random layers interstratifications exhibiting two hydration states (0W and 1W). The first contribution is dominated by 1W phases and the second one contains a few amounts of 0W layers. Even at **50% RH**, the structure is reproduced using two contributions related, respectively, to 1W:0W ratio with 80:20 and 1W:0W ratio with 35:65. From **40** to **20% RH**, samples present in total (1W:0W ratio with 68.5: 31.5), (1W:0W ratio with 67.4:32.6), and (1W:0W ratio with 62.5:37.5) attributed, respectively, to 40, **30,** and **20% RH**. For extreme desiccated conditions (**10% RH),** the structure is characterized by a high MLS number. Indeed, sample is characterized by a dominance of dehydrated layers with the highest proportion of 0W (67%) at the expense of the monohydrated layer 1W (33%). The relative proportions of different mixed layer structures and their compositions used in modelling are reported in Table 6.

Hydration process: In spite of the steadily increasing of RH conditions to 40% RH, quantitative analysis shows that the 0W layer persists with a major proportion. All XRD patterns are fitted assuming the presence of two MLS. Up to 6**0% RH**, the optimum structure model determined for SbId-1-Cs, include two interstratified structures with various proportions of 0W and 1W layers. The obtained model shows that the increase of RH rate is accompanied by an augment of the monohydrated layer proportion to the detriment of dehydrated layers. From 70 **to 80% RH,** the Theoretical model shows that the 1W layers dominate the main structure. Optimum structural parameters used to fit XRD profiles are summarized in Table 6.

3.2.2.2. SWy-2-Cs investigation. Qualitative XRD analysis: The obtained XRD patterns related to **SWy-2-Cs** smectite showed that overall the investigated RH field, all *001* picks is characterized by a symmetric profile geometry (Fig. 8) which indicates a homogenous hydrated state, whereas the high FWHM and ξ parameter value (Table 3) and the irrationality of the *00l* reflection positions, at the high and the low RH values, indicate probably an interstratified character. The evolution of the *001* reflection is very slow over all RH ranges (Fig. 4) and the d_{001} value does not exceed 13.13 Å. In both dehydration-hydration processes the smectite crystallite is dominated by the monohydrated layer types except at the high RH values (80% RH), where structure present an intermediate hydration state (1W–2W).

Quantitative XRD analysis. Dehydration process: From 80 to 60% RH, the theoretical structure is described using three MLS configurations randomly distributed. The decreasing of the RH rate is accompanied by a progressive declining of the relative 2W layers

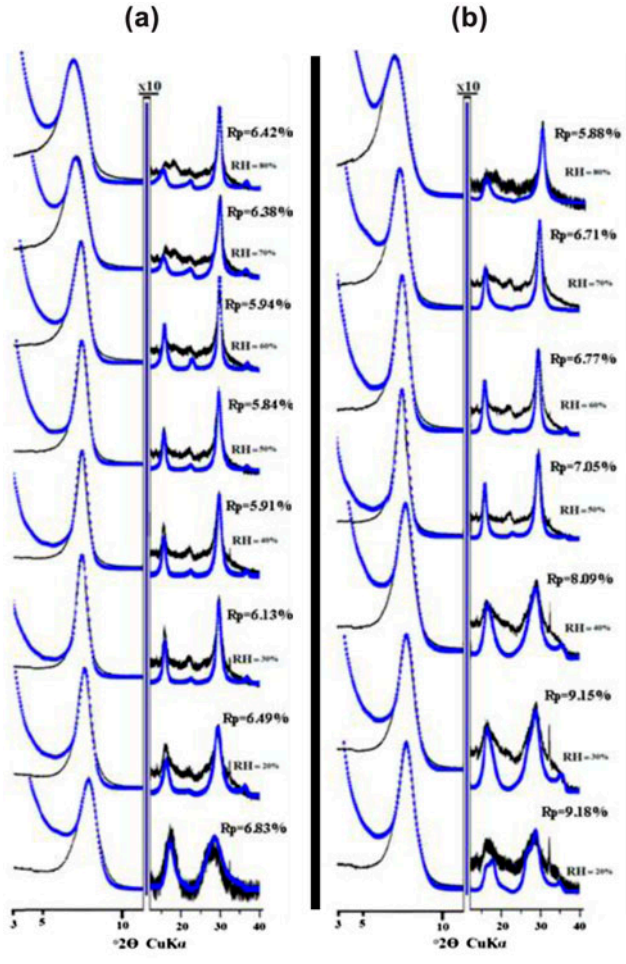

Fig. 8. Best agreement between theoretical (****) and experimental (——) XRD pattern for all measured %RH along the dehydration (a) and hydration (b) process of SWy-2-Cs.

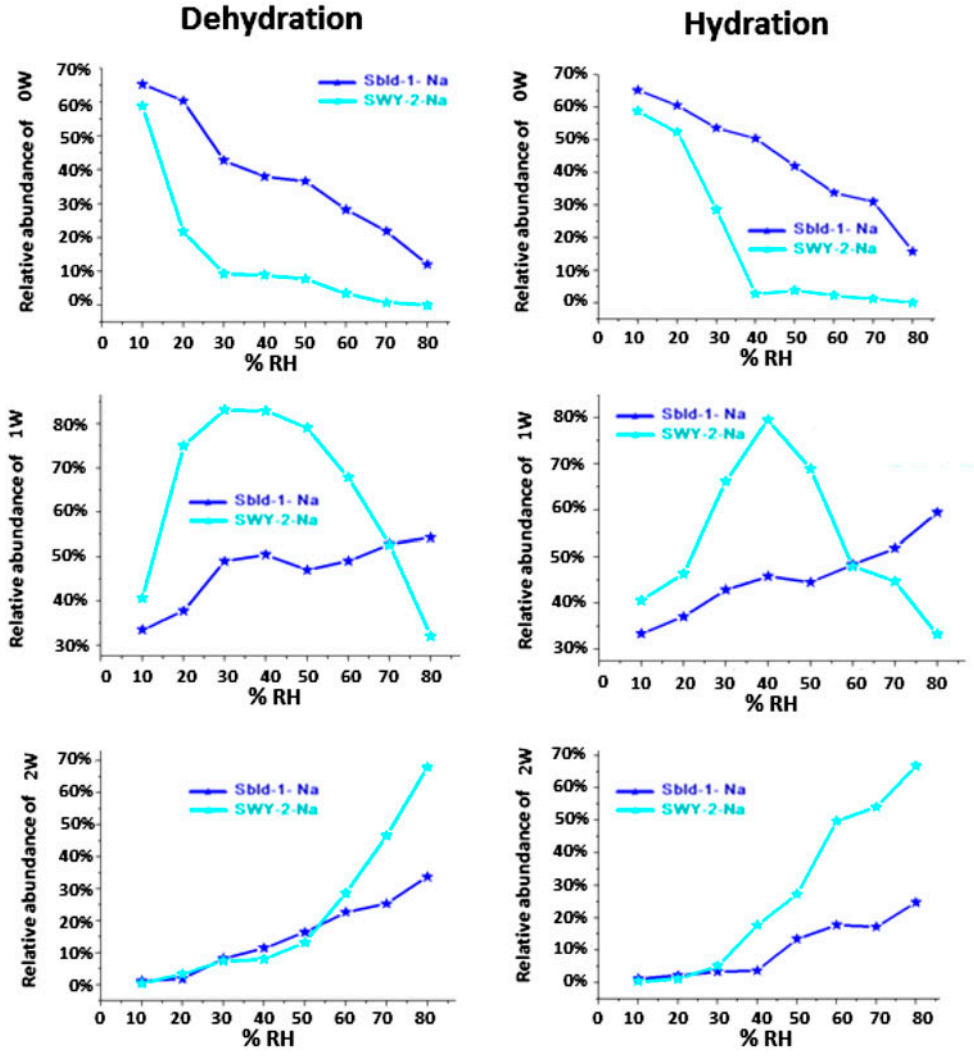

Fig. 9. Relative contribution of the different layer types (0W, 1W, and 2W) as function of %RH rates along the dehydration–hydration process. Case of SWY-2-Na and SbId-1-Na.

amount. At **50% RH**, the best fit is achieved using one MLS configuration including a significant proportion of 1W layers (85%) with a few proportion of 0W layers (15%) randomly distributed. The number of layers per stack is 8. The best agreement obtained between theoretical and experimental profiles recorded at **40 to 20% RH** is achieved using one MLS with different proportion of monohydrated and dehydrated layers randomly distributed. The relative abundances of these two types of layers are (1W:0W ratio 82:18), (1W:0W ratio 80:20), and (1W:0W ratio 65:35), respectively, for 40, 30, and 20% RH. The modeling of the experimental XRD patterns recorded at the extremely dry conditions **(10%RH)** showed interstratifications between 0W and 1W layer hydration state with a major contribution of the dehydrated layer (1W:0W ratio 45:55). All structural parameters that made it possible to have these agreements are summarized in Table 7.

Hydration process: To satisfactorily reproduce the experimental positions and profiles of 001 reflections, from **10 to 20%RH**, two contributions, including different proportions of 0W and 1W layers, are used. The first MLS is composed by (1W:0W) ratio with (15:85) abundance and the second one contains (1W:0W) ratio with 60:40.

At **30** and **40% RH**, the structure is characterized by two populations including 1W and 0W layers. For **50% RH**, the experimental XRD patterns is reproduced using a single structure exhibiting 80% of monohydrated layer (1W) and 20% of dehydrated ones randomly distributed. From **60** to **70% RH**, the experimental XRD patterns are reproduced using a just one MLS exhibiting 1Wand 0W with a major proportion

for the monohydrated layer. The 1W-2W transition is observed at the high RH rate (**80% RH)** characterized by an increase of the MLSs number. The total structure contains a major contribution of 1W layer (79.5%), 16.5% of 0W, and a few proportions for 2W phases (4%). The structural parameters that made it possible to have these agreements are summarized in Table 7.

4. Discussion

4.1. Relation between hydration heterogeneities and the number of mixed layer structure

Removal of cesium from aqueous solutions represents one of the topics that many studies are widely focused based on different methods. In this respect, [47] studied the efficiency of aluminum-pillared montmorillonite (PILMs) on the removal of cesium from aqueous solutions, where the main results reported that the kinetic studies shows an equilibrium time of a few minutes was needed for the adsorption of metal ions on PILMs and that cesium sorption isotherms were best represented by a two-site Langmuir model. Furthermore, **[**48] use batch and radioactive tracer technique to measure the distribution coefficients of cesium on natural and cation-enriched (Na^{+}, K^{+}, NH^{4+}, and Ca^{+2}) forms of clinoptilolite where the fit is achieved by Langmuir, Freundlich, and Dubinin–Radushkevich (D–R) models proving a breakthrough behavior of cesium on natural and cation-enriched forms of clinoptilolite for a particular set of conditions were also determined in a small-sized column.

In this work, the hydration behavior of Cs and Na exchanged smectite is studied after having undergone one dehydration–hydration cycle. Indeed, several former works focus similar studies while being based on XRD investigations. Ferrage et al. [21], demonstrate in the case of high-charge montmorillonite (i.e. SAz-1) and low-/high-charge beidellites (i.e. SbId-1 and Sb-Ca), studied under controlled atmosphere and saturated by Sr and Ca cation, that structure models are more heterogeneous for beidellite than for montmorillonite. They also show that the increase of the hydration heterogeneity in beidellite originates from the presence of 0W (nonexpandable) and of 1W layers under high RH conditions. Through this study, the proposed theoretical models used to fit beidellite specimen are more heterogeneous and present more complex structure in "crystallite" characterized by numerous contributions of MLSs than those used in the case of montmorillonite, along the dehydration–hydration cycle. This result is in accordance with earlier study, especially in term of structures heterogeneities. Indeed, for SbId-1-Na sample, and along dehydration process, the structure is characterized by fours MLSs contributions including different relative proportion of the three layer types (0W, 1W, and 2W). The maximum structural heterogeneity is observed with increasing RH rate to 20% RH where structure presents five layer types dominated by the dehydrated layers (0W); the lowest heterogeneity is observed, near to the room condition, at 50% RH, whereas at 80% RH, along the hydration process, theoretical model include just two MLSs types. For SbId-1-Cs sample, over all dehydration process, the structure is described using two MLSs contributions composed of two hydration states (0W and 1W) types. On the other hand, the gradual evolution of the relative proportion, related to the dehydrated and monohydrated layers, is relatively slow vs. decreasing RH rate. Along the hydration process, the most heterogeneous hydration behavior is observed between 20 and 40% RH where the number of MLSs used to fit experimental data increases to three MLS contributions. In the case of Na and Cs exchanged montmorillonite, quantitative investigation reveals that the hydration heterogeneities level varied with RH conditions. Indeed, hydration heterogeneities increase with the RH rate and the structure is described using three MLSs types including three hydrated layer types (i.e. 2W, 1W, and 0W) for ($60\% \leq RH \leq 80\%$). From 50% to the extremely dry condition (10%RH), heterogeneity decrease and the bihydrated layers disappeared from structure.

4.2. Hydration heterogeneities origin: charge location and ionic radius

4.2.1. Effect of Ionic radius

The observed hydration heterogeneities in the case of Na and Cs saturated specimen can be interpreted by the ionic radius effect which induces a different water affinity for the exchangeable cation. Indeed, the comparison of the relative abundance evolution of different layer types between **SWy-2-Na** and **SWy-2-Cs**, as a function of RH rates shows that the relative abundance of dehydrated layers (i.e. 0W) is much more important in the case of **SWy-2-Cs** samples than **SWy-2-Na** along the dehydration-hydration process. For **SWy-2-Na complex** (Fig. 9)**,** the increasing of the RH rate, during the hydration process, is accompanied by a fast and a significant decreasing of 0W layers beginning from 20% RH and continued to 40%RH where the dehydrated layers proportion shift to 2.75% and maintain a lower amount towards high RH condition. Whereas for **SWy-2-Cs** (Fig. 10), a notable decrease of the relative abundance of 0W layers is started at 50%

RH and continued to 80% RH with a proportion around 15%. The comparison of the relative contribution of the monohydrated layer (i.e. 1W) between the two samples shows a fast and continued shift in the progress of this layer types populations as a function as % RH condition along the hysteresis cycle especially for **SWy-2-Na**. At high RH rate, the **SWy-2-Cs** keeps the uppermost proportions of 1W layers. The most important proportion of 2W layers is noted for **SWy-2-Na** complex , whereas **the SWy-2-Cs** present a small amount that does not exceed 4% at the high RH condition, in hydration process and 15.5% in the dehydration process. Figs. 9 and 10 display the relative layer type abundances evolution as a function of % RH over the dehydration–hydration process, in the case of SbId**-1-Na** and **SbId-1-Cs** samples**.** We show that at the high RH rate, the **SbId-1-Cs complex** has the highest proportion of dehydrated layer (31.25%) comparing to **SbId-1-Na** (15.75%). By decreasing %RH value, the relative proportion of 0W layers decreases so slowly **from the** structure of **SbId-1-Cs** and it remains almost constant turning around 30% from 80 to 30% RH. Whereas the decreasing of 0W layers abundance along the dehydration process is faster for **SbId-1-Na.** On the other hand, along the hydration process, the relative abundance of 0W layers of **SbId-1-Cs** decreases slower than **SbId-1-Na**, and it maintains the elevated proportion from 30 to 80%RH. For the monohydrated layer, the **SbId-1-Cs** have the maximum relative proportion throughout all studied %RH ranges, whereas, it has unfounded proportion of the bihydrated layers (i.e. 2W) along the dehydration–hydration cycle. As a conclusion, the beidellite present more complex structure characterized by an elevated number of MLS contributions than the montmorillonite in both dehydration and hydration process. Also, the presence of Cs cation in the interlamellar space induces heterogeneous hydration character.

4.2.2. Effect of charge location

Several authors [22,49,50] investigate the effect of exchangeable cation nature on the swelling properties of dioctahedral and/or trioctahedral smectite. Oueslati et al. [22] studied the hydration properties of reduced-charge montmorillonitesseries, saturated by several metallic cation, using *in situ* XRD analysis at different RHs. They demonstrate that the decrease of the negative charge on the layers had a minor effect on the water uptake at all investigated RHs. Ferrage et al. [50] studied the influence of layer charge and charge location on the hydration properties of dioctahedral smectite. Where they demonstrate that distribution of layers with different hydration states (dehydrated—0W, monohydrated—1W, bihydrated—2W, or tri-hydrated—3W) within smectite crystals often leads to two distinct contributions to the XRD pattern, each contribution having different layer types randomly interstratified. In order to assess the effect of the charge location on the hydration behavior of different samples, the evolution of the relative proportion of different layer types (0W, 1W, and 2W) as a function of RH is compared between the octahedral substituted charge (SWY-2) and the tetrahedral substituted ones (SbId-1) saturated at the first time with Na^+, then saturated with Cs^+ cations.

4.2.2.1. Na-saturated specimen. The relative proportions of different hydrations states (0W, 1W, and 2W), respectively, for SWy-2-Na and SbId-1-Na sample are presented in Fig. 9. This comparison showed that all over the dehydration-hydration process, the Na-saturated beidellite has much more important relative proportion of 0W layers than Na-saturated montmorillonite. The beidellite sample keeps a high 0W layer proportion even at the uppermost rate of RH condition (15.75% in the hydration sequence and 12% in dehydration sequence). Whereas the dehydrated layers (i.e. 0W) were completely disappeared from the montmorillonite structure at 80% RH. For 1W layer hydration state, we showed, along the dehydration process, that the relative proportion of the monohydrated layers of SbId-1-Na decrease slowly with RH rates, while SWy-2-Na present two different hydration behaviors respectively from 10 to 40%RH and 40 to 80%RH. All over the dehydration–hydration cycle, the **SWy-2-Na** present a main relative proportion of the bihydrated layers (i.e. 2W) compared to **SbId-Na** complex at different RH condition.

4.2.2.2. Cs-saturated specimen. The evolution of different hydration state contribution of **SWy-2-Cs** and **SbId-1-Cs** are illustrated in Fig. 10. The comparison of the relative abundance of the dehydrated layers (i.e. 0W) shows that, the nonexpandable layers are mostly present in the structure of **Cs-saturated beidellite** more than in the case of **Cs-saturated montmorillonite** along the dehydration and hydration process. In addition **SbId-1-Cs** complex retains a high proportion of 0W layers at high % RH rate. For the monohydrated layers (i.e. 1W), **SWy-2-Cs** complex preserves high 1W layer abundance. Finally, the evolution of the relative proportion of the bihydrated layers indicates that **SbId-1-Cs** sample does not exhibit this hydration layer type in the structure along the hydration and dehydration process. For **SWy-2-Cs sample**, the 2W phases disappear completely from structure at 50% RH in dehydration sequaence and appeared again just

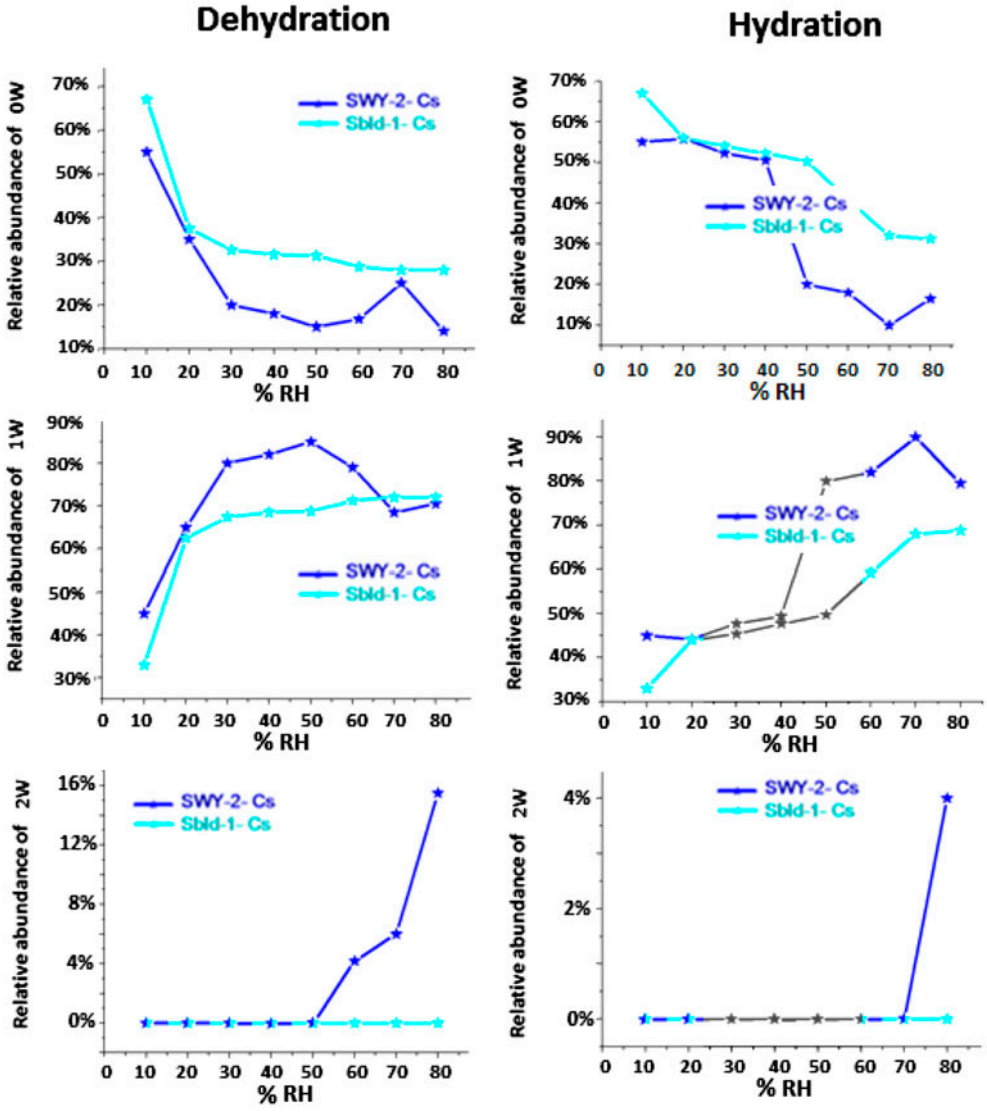

Fig. 10. Relative contribution of the different layer types (0W, 1W and 2W) as function of %RH rates along the dehydration–hydration process. Case of SWY-2-Cs and SbId-1- Cs.

at high RH rate along the hydration process (80% RH).

Summarily, the effect of the location charge on the hydration behavior for the studied smectite can be detected throughout the dehydration–hydration cycle in particular at the high %RH value. Indeed the attractive forces between adjacent 2:1 layers and interlayer cations restrict the penetration of the H_2O molecule in interlamellar spaces and limits the hydration "growth" at 2W hydration state .Which can be explained by the important relative proportion of dehydrated layers even at high RH rate for the smectites with tetrahedral deficit charge (SbId-1-Cs, SbId-1-Na) and the total absence of dehydrated layers (i.e. 2W), from their structure in hydration and dehydration process.

5. Conclusion

The present work is based on the XRD profile modeling method in order to study the hydration behavior, of dioctahedral smectites, as a function of RH along the dehydration–hydration cycle. This method allowed us to study the structure heterogeneities degree affected by the ionic radius of exchangeable cation and the charge location of the host materials. The obtained results showed that:

(1) Overall, the dehydration and hydration process, the structure of Na^+ and/or Cs^+ saturated beidellite is characterized by a heterogeneous hydration state and presents numerous contributions of MLSs at the crystal scale more than those used for Na^+ and/or Cs^+ saturated montmorillonite specimens.
(2) The investigation of MLSs content shows that the presence of Cs^+ cations in exchangeable sites is accompanied by a decrease of the hydration heterogeneities degree in smectite "crystallite", thus the Cs-saturated samples present a MLSs number lower than in the case of samples saturates with Na^+ cations.
(3) The theoretical models related to the Cs-saturated smectites present a main structure with a major contribution of 0W and 1W layers. Whereas in the case of Na-saturated samples, the structure models obtained at different RH rates, are characterized by the presence of three layer types (0W, 1W, and 2W) with different relative proportion. Therefore the presence of Cs^+ cation, characterized by its huge size, in exchangeable sites limit the opening of interlayer spaces and the insertion of H_2O molecules which prevent the 1W–2W transition at high RH rate in both hydration and dehydration procedure .
(4) The deficit charge origin is also an important intrinsic property which influences the hydration behavior. Indeed, the tetrahedral charge location, contribute to increase attractive force between cation and the 2:1 layers which prevent the 1W-2W transition. This may explain the dominance, in term of abundance, of 0W and 1W layer types. This result is confirmed for SbId-1-Cs and SbId-1-Na (tetrahedral-substituted charge) samples which are described by the upper proportion of dehydrated and monohydrated layers, compared to SWy-2-Cs and SWy-2-Na (octahedral-substituted charge), where MLSs show the coexistence of 2W, 1W, and 0W layers at the crystal scale throughout the dehydration and hydration process.

Acknowledgments

The results presented are a part of a PhD thesis realized at the PMLNMH (UR05/13-01)-Faculty of science of bizerte, Co-supervised by Dr W. Oueslati and Prof. Abdesslem Ben Haj Amara. Marwa Ammar acknowledges Walid Oueslati for the fruitful discussions about smectite hydration, her main contribution in the XRD modeling approach and the proof readings of the manuscript. The content and style of the paper greatly benefited from comments of anonymous reviewers and those of the editor.

References

[1] G. Rytwo, R. Lavi, Y. Rytwo, H. Monchase, S. Dultz, T.N. König, Clarification of olive mill and winery wastewater by means of clay-polymer nanocomposites, Sci. Total Environ. 442 (2013) 134–142.
[2] G. Rytwo, The use of clay–polymer nanocomposites in wastewater pretreatment, Scient. World J., 2012 (2012) Article ID 498503.
[3] G.W. Brindley, G. Brown, Crystal Structures of Clay Minerals and their X-ray Identification, Miner. Soc, London,. pp. 125–195, 1980.
[4] W.F. Bleam, Atomic theories of phyllosilicates: Quantum chemistry, statistical mechanics, electrostatic theory, and crystal chemistry, Rev. Geophys. 31 (1993) 51–74.
[5] R.E. Grim, Applied Clay Mineralogy, McGraw-Hill Book, New York, p. 422, 1962.
[6] E.S. Boek, P.V. Coveney, N.T. Skipper, Monte Carlo molecular modelling studies of hydrated Li^-, Na^-, and K smectites: understanding the role of potassium as a clay swelling inhibitor, J. ACS 117 (1995) 12608–12617.
[7] S. Karaborni, B. Smit, W. Heidug, J. Urai, E. Van Oort, The swelling of clays: molecular simulations of the hydration of montmorillonite, Science 271 (1996) 1102–1104.
[8] S. Çoruh, F. Geyikçi, Adsorption of copper (II) ions on montmorillonite and sepiolite clays: Equilibrium and kinetic studies, Desalin. Water Treat. 45 (2012) 351–360.
[9] Q. Yang, J. Zhang, Q. Yang, Y. Yu, G. Yang, Behavior and mechanism of Cd(II) adsorption on loess-modified clay liner, Desalin. Water Treat. 39 (2012) 10–20.
[10] N.T. Skipper, F.-R.C. Chang, G. Sposito, Monte Carlo simulation of interlayer molecular structure in swelling clay minerals. 2. Monolayer hydrates, Clays Clay Miner. 43 (1995) 294–303.
[11] W. Oueslati, M. Meftah, H. Ben Rhaiem, A. Ben Haj Amara, Selectivity of Na-montmorillonite versus concentration of two competitive bivalent cations (Cu^{2+}, Pb^{2+}): quantitative XRD investigation, Adv. Mat. Sci. Eng. (2009), Article ID 385673.
[12] N.T. Skipper, P.A. Lock, J.O. Titiloye, J. Swenson, Z.A. Mirza, W.S. Howells, F. Fernandez-Alonso, The structure and dynamics of 2-dimensional fluids in swelling clays, Chem. Geol. 230 (2006) 182–196.
[13] M. Zamparas, Y. Deligiannakis, I. Zacharias, Phosphate adsorption from natural waters and evaluation of sediment capping using modified clays, Desalin. Water Treat. 51(13–15) (2013) 2895–2902.
[14] J.Q. Jiang, Z. Zeng, P. Pearce, Preparation and use of modified clay coagulants for wastewater treatment, Water, Air, Soil Pollut. 158 (2004) 53–65.
[15] N. Malikova, V. Marrya, J.-F. Dufrechea, P. Turqa, Na/Cs montmorillonite: Temperature activation of diffusion by simulation, Curr. Opin. Colloid Interface Sci. 9 (2004) 124–127.
[16] S.W. Zhou, M.G. Xu, Y.B. Ma, S.B. Chen, D.P. Wei, Aging mechanism of copper added to bentonites, Geod 147 (2008) 1–2.
[17] X. Liu, R. Wang, H. Zhou, Effects of layer-charge distribution on the thermodynamic and microscopic properties of Cs-smectite, Geochim. Cosmochim. Acta 72 (2008) 1837–1847.
[18] J.M. Cases, I. Berend, G. Besson, M. Francois, J.P. Uriot, F. Thomas, J.E. Poirier, Mechanism of adsorption and desorption of water vapor by homoionic montmorillonite. 1. The sodium exchanged form, Langmuir 8(11) (1992) 2730–2739.
[19] I. Bérend, J.M. Cases, M. François, J.P. Uriot, L.J. Michot, A. Masion, F. Thomas, Mechanism of adsorption and desorption of water vapour by homoionic montmorillonites. 2. The Li^+, Na^+, K^+, Rb^+ and Cs^+ exchanged forms, Clays Clay Miner. 43 (1995) 324–336.

[20] J.M. Cases, I. Bérend, M. François, J.P. Uriot, L.J. Michot, F. Thomas, Mechanism of adsorption and desorption of water vapour by homoionic montmorillonite. 3. The Mg^{2+}, Ca^{2+}, Sr^{2+} and Ba^{2+} exchanged forms, Clays Clay Miner. 45 (1997) 8–22.
[21] E. Ferrage, B. Lanson, B.A. Sakharov, V.A. Drits, Investigation of smectite hydration properties by modeling of X-ray diffraction profiles. Part1. Montmorillonite hydration properties, Am. Mineral. 90 (2005) 1358–1374.
[22] W. Oueslati, M.S. Karmous, H. Ben Rhaiem, B. Lanson, A. Ben Haj Amara, Effect of interlayer cation and relative humidity on the hydration properties of a dioctahedral smectite, Z. Kristallogr. Suppl. 26 (2007) 417–422.
[23] T. Sato, T. Watanabe, R. Otsuka, Effects of layer charge, charge location, and energy change on expansion properties of dioctahedral smectites, Clays Clay Miner. 40 (1992) 103–113.
[24] W.F. Moll, Baseline studies of the clay mineral society source clays: Geological origin, Clays Clay Miner. 49 (2001) 374–380.
[25] J.L. Post, B.L. Cupp, F.T. Madsen, Beidellite and associated clays from the DeLamar mine and Florida Mountain area, Idaho, Clays Clay Miner. 45 (1997) 240–250.
[26] H. Gaboriau, Interstratifiés Smectite-Kaolinite de l'Eure. Relation entre la structure, la texture et les propriétés en fonderie, Thèse Université d'Orléans, France, 1991, p. 273.
[27] D. Tessier, Experimental study of the clay materials organization. Hydration, swelling and structure along drying and re-wetting, thesis University of Paris VII, France, Publication INRA Versailles, 1984.
[28] J. Srodon, D.J. Morgan, E.V. Eslinger, D.D. Eberl, M.R. Karlinger, Chemistry of illite/smectite and end-member illite, Clays Clay Miner. 34 (1986) 368–378.
[29] S.W. Bailey, Nomenclature for regular interstratifications, Am. Miner. 67 (1982) 394–398.
[30] B.A. Sakharov, V.A. Drits, Mixed-layer kaolinte–montmorillonite: A comparison observed and calculated diffraction patterns, Clays Clay Miner. 21 (1973) 15–17.
[31] V.A. Drits, C. Tchoubar, X-ray Diffraction by Disordered Lamellar Structures: Theory and Applications to Microdivided Silicates and Carbons, Springer-Verlag, Berlin, p. 371 1990.
[32] V.A. Drits, B.A. Sakharov, X-ray Structure Analysis of Mixed-layer Minerals, Nauka, Moscow, 256 pp, 1976.
[33] W. Oueslati, H. Ben Rhaiem, A. Ben Haj Amara, XRD investigations of hydrated homoionic montmorillonite saturated by several heavy metal cations, Desalination 271 (2011) 139–149.
[34] W. Oueslati, H. Ben Rhaiem, A. Ben Haj Amara, Effect of relative humidity constraint on the metal exchanged montmorillonite performance: An XRD profile modeling approach, Appl. Surf. Sci. 261 (2012) 396–404.
[35] H. Ben Rhaiem, D. Tessier, A. Ben Haj Amara, Mineralogy of the 2 μm fraction of three mixed-layer clays from southern and central Tunisia, Clay Miner. 35 (2000) 375–381.
[36] J.A. Kittrick, Interlayer forces in montmorillonite and vermiculite, Soil Sci. Soc. Am. J. 33 (1969) 217–222.
[37] J.A. Kittrick, Quantitative evaluation of the strong-force model for expansion and contraction of vermiculite, Soil Sci. Soc. Am. J. 33 (1969) 222–225.
[38] D.A. Laird, Model for crystalline swelling of 2:1 phyllosilicates, Clays Clay Miner. 44 (1996) 553–559.
[39] D.A. Laird, Layer charge influences on the hydratation of expandle 2:1 phyllosilicates, Clays Clay Miner. 47 (1999) 630–636.
[40] H. Van Olphen, Thermodynamics of interlayer adsorption of water in clays, J. Colloid Sci. 20 (1965) 822–837.
[41] I. Berend, Hydration mechanisms of homoionic montmorillonites for less than 0.95 pressures, Doctoral thesis, INPL-Nancy, France, (1991) 330.
[42] T. Iwasaki, T. Watanabe, Distribution of Ca and Na ions in dioctahedral smectites and interstratified dioctahedral mica/smectites, Clays Clay Miner. 36 (1988) 73–82.
[43] D.M.C. MacEwan, M.J. Wilson, Interlayer and intercalation complexes of clay minerals: in: G.W. Brindley, G. Brown (Eds.), Crystal Structures of Clay Minerals and their X-ray Identification, Mineralogical Society, London, 1984, p. 197.
[44] D.M. Moore, J. Hower, Ordered interstratification of dehydrated and hydrated Na-smectite, Clays Clay Miner. 34 (1986) 379–384.
[45] T. Watanabe, T. Sato, Expansion characteristics of montmorillonite and saponite under various relative humidity conditions, Clay Sci. 7 (1988) 129–138.
[46] D. Karamanis, P.A. Assimakopoulos, Efficiency of aluminum-pillared montmorillonite on the removal of cesium and copper from aqueous solutions, Water Res. 41 (2007) 1897–1906.
[47] A. Abdelrahim, Y. Hayrettin, Removal of 137Cs from aqueous solutions using different cationic forms of a natural zeolite: clinoptilolite, Sep. Purif. Technol. 28 (2002) 103–116.
[48] J. Cuadros, Interlayer cation effects on the hydration state of smectite, Am. J. Sci. 297 (1997) 829–841.
[49] E. Ferrage, B. Lanson, B.A. Sakharov, N. Geoffroy, E. Jacquot, V.A. Drits, Investigation of dioctahedral smectite hydration properties by modeling of X-ray diffraction profiles: Influence of layer charge and charge location, Am. Miner. 92 (2007).